Downloaded from orbit.dtu.dk on: Mar 26, 2025

DTU Library

Reprogramming AA catabolism in CHO cells with CRISPR/Cas9 genome editing improves cell growth and reduces byproduct secretion

Ley, Daniel; Pereira, Sara; Pedersen, Lasse Ebdrup; Arnsdorf, Johnny; Hefzi, Hooman; Davy, Anne Mathilde; Kwang Ha, Tae; Wulff, Tune; Kildegaard, Helene Faustrup; Andersen, Mikael Rørdam

Published in:
Metabolic Engineering

Link to article, DOI:
10.1016/j.ymben.2019.09.005

Publication date:
2019

Document Version
Publisher's PDF, also known as Version of record

Link back to DTU Orbit

Citation (APA):
Ley, D., Pereira, S., Pedersen, L. E., Arnsdorf, J., Hefzi, H., Davy, A. M., Kwang Ha, T., Wulff, T., Kildegaard, H. F., & Andersen, M. R. (2019). Reprogramming AA catabolism in CHO cells with CRISPR/Cas9 genome editing improves cell growth and reduces byproduct secretion. *Metabolic Engineering*, *56*, 120-129. https://doi.org/10.1016/j.ymben.2019.09.005

General rights
Copyright and moral rights for the publications made accessible in the public portal are retained by the authors and/or other copyright owners and it is a condition of accessing publications that users recognise and abide by the legal requirements associated with these rights.

- Users may download and print one copy of any publication from the public portal for the purpose of private study or research.
- You may not further distribute the material or use it for any profit-making activity or commercial gain
- You may freely distribute the URL identifying the publication in the public portal

If you believe that this document breaches copyright please contact us providing details, and we will remove access to the work immediately and investigate your claim.

Metabolic Engineering 56 (2019) 120–129

Contents lists available at ScienceDirect

Metabolic Engineering

journal homepage: www.elsevier.com/locate/meteng

Reprogramming AA catabolism in CHO cells with CRISPR/Cas9 genome editing improves cell growth and reduces byproduct secretion

Daniel Ley[a,b], Sara Pereira[b], Lasse Ebdrup Pedersen[b], Johnny Arnsdorf[b], Hooman Hefzi[c,d], Anne Mathilde Davy[a], Tae Kwang Ha[b], Tune Wulff[b], Helene Faustrup Kildegaard[b], Mikael Rørdam Andersen[a,*]

[a] Department of Biotechnology and Biomedicine, Technical University of Denmark, Kgs. Lyngby, Denmark
[b] The Novo Nordisk Foundation Center for Biosustainability, Technical University of Denmark, Kgs. Lyngby, Denmark
[c] Department of Bioengineering, University of California, San Diego, La Jolla, CA, 92093, United States
[d] Novo Nordisk Foundation Center for Biosustainability at the University of California, San Diego, School of Medicine, La Jolla, CA, 92093, United States

ARTICLE INFO

Keywords:
Chinese hamster ovary cells
Lactate
Ammonium
AA catabolism
CRISPR
Metabolic network reconstruction

ABSTRACT

Chinese hamster ovary (CHO) cells are the preferred host for producing biopharmaceuticals. Amino acids are biologically important precursors for CHO metabolism; they serve as building blocks for proteogenesis, including synthesis of biomass and recombinant proteins, and are utilized for growth and cellular maintenance. In this work, we studied the physiological impact of disrupting a range of amino acid catabolic pathways in CHO cells. We aimed to reduce secretion of growth inhibiting metabolic by-products derived from amino acid catabolism including lactate and ammonium. To achieve this, we engineered nine genes in seven different amino acid catabolic pathways using the CRISPR-Cas9 genome editing system. For identification of target genes, we used a metabolic network reconstruction of amino acid catabolism to follow transcriptional changes in response to antibody production, which revealed candidate genes for disruption. We found that disruption of single amino acid catabolic genes reduced specific lactate and ammonium secretion while specific growth rate and integral of viable cell density were increased in many cases. Of particular interest were *Hpd* and *Gad2* disruptions, which show unchanged AA uptake rates, while having growth rates increased up to 19%, and integral of viable cell density as much as 50% higher, and up to 26% decrease in specific ammonium production and to a lesser extent (up to 22%) decrease in lactate production. This study demonstrates the broad potential of engineering amino acid catabolism in CHO cells to achieve improved phenotypes for bioprocessing.

1. Introduction

Chinese hamster ovary (CHO) cells are the predominant cell factory for producing recombinant therapeutic proteins, a segment of the pharmaceutical industry worth more than 188 billion USD in 2017 alone (Walsh, 2018). A key element for improving CHO-based production of active pharmaceutical ingredients (APIs) has traditionally been the development of optimized growth media that provide cells with excess nutrients to support growth and protein productivity. Today, fed-batch bioprocessing of CHO cells is complicated by accumulation of toxic metabolic by-products, mainly lactate and ammonium, which inhibit growth (Lao and Toth, 1997), impair recombinant protein quality (Andersen and Goochee, 1995; Borys et al., 1994; Thorens and Vassalli, 1986; Yang and Butler, 2000), and productivity (Hansen and Emborg, 1994). To address this problem, bioprocessing- and cell line engineering efforts have mainly targeted glucose and glutamine metabolism (reviewed by Ahn and Antoniewicz, 2012; Altamirano et al., 2013; Young, 2013). However, the impact of amino acid (AA) catabolism on lactate and ammonium production has received less attention, despite the fact that AA catabolism is directly linked to ammonium production, and indirectly, through redox metabolism, to lactate production. This prompted us to study the physiological effects of reprogramming AA catabolism in CHO cells. Specifically, the physiological impact of disrupting AA catabolic pathways, and in particular, the allocation of AAs to catabolism and biomass synthesis.

AA catabolism is in many ways an unwanted process in a CHO cell producing a biopharmaceutical. For one, the AAs would be more efficiently used directly in protein biosynthesis and biomass production. AA catabolism generates ammonium by transamination, a chemical reaction that transfers an amino group to α-ketoglutarate to form

* Corresponding author. Søltofts plads, bygning 223, 2800, Kgs Lyngby, Denmark.
E-mail address: mr@bio.dtu.dk (M.R. Andersen).

https://doi.org/10.1016/j.ymben.2019.09.005
Received 4 April 2019; Received in revised form 10 August 2019; Accepted 10 September 2019
Available online 14 September 2019
1096-7176/ © 2019 The Authors. Published by Elsevier Inc. on behalf of International Metabolic Engineering Society. This is an open access article under the CC BY-NC-ND license (http://creativecommons.org/licenses/BY-NC-ND/4.0/).

glutamate, which is deaminated to yield ammonium (Ahn and Antoniewicz, 2012). AA catabolism contributes to lactate production as well, either directly by fueling carbon to glycolysis (Templeton et al., 2014), or in an indirect redox-dependent manner. Many AA catabolic pathways reduce NAD^+ to NADH, which perturb the redox equilibrium, and force the cell to regenerate cytosolic NAD^+ pools through lactate synthesis, to maintain redox homeostasis (Templeton et al., 2014). So far, only a single study (Mulukutla et al., 2019) has been published targeting AA catabolism (excluding glutamine) in CHO cells, despite these pathways accounting for 25% of the total carbon pool fueling central carbon metabolism (Nicolae et al., 2014).

Recent evidence suggests that AA catabolism in CHO cells produces a wide range of growth-inhibiting compounds besides lactate and ammonium. Mulukutla et al., 2017 identified nine growth-inhibiting compounds from catabolism of phenylalanine, tyrosine, tryptophan, methionine, leucine, serine, threonine and glycine. They patented that controlling these AAs at low concentrations reduced inhibitor accumulation and improved peak cell density and antibody titers in fed-batch culture (Hiller and Mulukutla, 2017, 2015). Similarly, González-Leal et al. (2011) found that leucine and threonine inhibit peak cell density and maximum specific growth rate during exponential growth, and suggested a feeding strategy, in which these AAs remain at sufficiently low concentrations, to avoid growth inhibiting effects while sustaining protein synthesis. Clinical studies provide several indications that intermediates in AA catabolism are toxic to mammalian cells in general, and thus may be growth-inhibiting in CHO cells: Sallée et al. (2014) identified toxic AA catabolites in the primary catabolic pathway of tryptophan, the kynurenine pathway. Beltrán-Valero de Bernabé et al. (1999) and Rodríguez et al. (2000) found toxic intermediates in the common catabolic pathway of tyrosine and phenylalanine. Additionally, Hallen et al. (2013) suggest that the main catabolic pathway of lysine, the saccharopine pathway, produces reactive aldehydes that are potentially toxic, as they form adducts and condensation products with proteins and DNA. In combination, these studies highlight a broad range of potentially detrimental activities associated with AA catabolism in CHO bioprocessing.

To address the impact of AA catabolism on CHO cell physiology in a progressive manner, we devised a rational genetic engineering strategy to study the physiological response to disruption of individual AA catabolic pathways before proceeding to disrupt multiple pathways in concert. For selection of target genes, we utilized a network reconstruction of AA catabolism in CHO cells to follow transcriptomic changes in AA catabolic pathways in response to protein production, which provided a rational basis for disrupting genes using the RNA-guided Cas9 nuclease. We monitored physiological changes in terms of maximum specific growth rate (μ_{max}), integral of viable cell density (IVCD), and major exo-metabolite secretion in parallel shake flask and bioreactor cultures. Our data contribute to the fundamental understanding of AA catabolism in relation to CHO-based bioprocessing, and highlight the applicability of rational cell line engineering strategies to reduce endogenous production of toxins derived from catabolism of AAs.

2. Materials and methods

2.1. RNA seq data generation

Three CHO cell lines; two expressing a recombinant human IgG and one not expressing any recombinant protein (Lund et al., 2017), were cultivated in batch mode in 125 mL shake flasks (Corning). Note that these cell lines were not used in the engineering and cultivation studies; see details below for these. RNA was extracted when the cells were in exponential growth phase and in stationary phase. RNA-seq was performed by Multiplexed cDNA library generation using the TruSeq RNA Sample Preparation Kit v2 (Illumina, Inc., San Diego, CA) and next-generation sequencing were performed by AROS Applied Biotechnology (Aarhus, Denmark) using eight samples per lane in an Illumina Hiseq 2000 system for paired-end sequencing (SRA accession: SRP073484) as described previously (Lund et al., 2017). RNA-Seq data were processed as described by Lund et al. (2017) and trimmed reads were mapped to the CHO-K1 genome (assembly and annotation) released in 2014 (NCBI Accession: GCF_000223151.1) using TopHat2 version 2.0.9 (using Bowtie 2.2.0) with default settings (Kim et al., 2013; Langmead et al., 2009). Read counts for each transcript were obtained with HTSeq count version 0.5.4p3 using the intersection none-empty mode (Anders et al., 2015). The read counts were normalized using EdgeR (version 3.6.8) (Robinson et al., 2010) in R (Ihaka and Gentleman, 1996). Genes with detected counts per million in less than two samples were disregarded. Differential analyses were performed using the GLM likelihood ratio test in EdgeR for the experiments with multiple factors. A p-value of 0.05 and a false discovery rate < 0.05 as well as $\pm$ log2.0 fold changes were used as the default thresholds to identify the differentially expressed genes.

2.2. Metabolic network reconstruction

For integration of transcriptomic data and selection of target genes for genome editing, we employed a CHO-specific metabolic network reconstruction of glycolysis and AA catabolism as described previously (Ley et al., 2015). Briefly, a metabolic network reconstruction of glycolysis and AA catabolism in CHO cells was generated using mouse genomic and biochemical pathway information from the KEGG database (Kanehisa and Goto, 2000) as a starting point. To identify orthologous metabolic genes in CHO, a protein BLAST search of AA metabolic genes from mouse was conducted against the CHO-K1 genome (Xu et al., 2011), hosted at http://www.CHOgenome.org (Hammond et al., 2012). The resulting list of CHO genes was manually curated for inclusion based on information from literature. The finalized reconstruction features 319 proteins catalyzing 183 reactions with 188 metabolites.

2.3. Single-guide RNA target design, transfection, single cell sorting and genotype verification

Design and selection of single-guide RNA (sgRNA) target sites was performed with the online tool “CRISPy” (Ronda et al., 2014). The sgRNA expression vectors were constructed as previously described by Ronda et al. (2014). Prior to transfection, CHO-S suspension cells obtained from Life Technologies were grown in CD-CHO medium (Thermo Fisher Scientific, Waltham, MA, USA) supplemented with 8 mM L-glutamine (Life Technologies) and 0.2% anti-clumping reagent (Life Technologies) in a humidified shaking incubator operated at 37 °C, 5% CO_2 and 120 rpm. One day prior to transfection, cells were washed and seeded in medium without anti-clumping reagent at 5×10^5 cells/mL. Cells were transfected with expression vectors encoding Cas9 nuclease linked to GFP via a 2A peptide (GFP_2A_Cas9) as described by Grav et al. (2015), and sgRNAs targeting *Aass*, *Afmid*, *Ddc*, *Gad1*, *Gad2*, *Hpd*, *LOC100759874*, *Prodh* and *Prodh2* individually (See Table 1 for details), to generate single-gene knock out transfectants. For each sample, cell cultures with cell density of 1×10^6 cells/mL in 125 mL shake flasks (Corning), were transfected with 17.7 µg DNA using FreeStyle™ MAX reagent together with OptiPRO SFM medium (Life Technologies), according to the manufacturers recommendations. For generation of multiple gene disruption transfectants, cells were co-transfected with equimolar amount of each plasmid encoding GFP_2A_Cas9 and selected sgRNAs, in a total of 17.7 µg expression vector DNA. Anti-clumping reagent (0.5%) was added one day after transfection. Two days subsequent to transfection, clones expressing GFP_2A_Cas9 were enriched from the population of transfectants, and single cell sorted using fluorescence activated cell sorting (FACS), as described by Grav et al. (2015). Single cell sorted clones were cultured in 96-well U bottom plates (BD Biosciences) for 14 days and genotypes were determined

Table 1
List of target genes, gene description, associated AA catabolic pathway and corresponding indel sizes.

Gene symbol	Gene ID	Protein names	Associated catabolic pathway	Indel sizes
Aass	100751161	Alpha-aminoadipic semialdehyde synthase	L-lysine	-1
Afmid	100773211	Kynurenine formamidase	L-tryptophan	+1
Ddc	100761742	Aromatic-L-amino-acid decarboxylase	L-tyrosine/L-phenylalanine	-29/-16
Gad1	100765882	Glutamate decarboxylase 1	L-glutamate	+28
Gad2	100757642	Glutamate decarboxylase 2	L-glutamate	-13
Hpd	100768220	4-hydroxyphenylpyruvate dioxygenase	L-tyrosine/L-phenylalanine	+1
LOC100759874	100759874	L-threonine 3-dehydrogenase	L-threonine	+1
Prodh	100750856	Proline dehydrogenase 1	L-proline	-20
Prodh2	100773901	Proline dehydrogenase 2	L-proline	-22

using deep sequencing analysis as described previously by Grav et al. (2015) (Miseq primers described in Supplementary Table 1).

2.4. Cell cultivation in shake flasks

Cultures were initiated from cryopreserved vials in preheated CD-CHO medium (Thermo Fisher Scientific) supplemented with 8 mM L-glutamine (Gibco) and 0.2% anti-clumping reagent (Gibco). Cells used were CHO-S cells (Life Technologies) as reference, and the engineered CHO-S-derived cells (See Table 1). Pre-cultures were passaged three times during a seven-day period prior to inoculation. To avoid cell aggregation, cells were passed through a 40 µm cell strainer (Sigma #CLS431750-50 EA) before inoculation. For characterization of single gene disrupted clones, cell culture was performed in 250 mL vented Erlenmeyer shake flasks (Corning, NY, USA) with a working volume of 80 mL in a humidified shaking incubator operated at 37 °C, 5% CO_2 and 120 rpm. For validation of physiological effects across multiple single gene disrupted clones, cell culture was performed in 125 mL vented Erlenmeyer shake flasks (Corning, NY, USA) with working volume of 40 mL, under similar conditions. All cultures were seeded at 3×10^5 viable cells/mL and grown for 6 days in batch culture. Samples were drawn daily and analyzed for cell density and culture viability using two methods: for the characterization of single gene disrupted clones we used the Nucleocounter NC-200 (Chemometec, Allerød, Denmark), while the for validation of physiological effects across multiple single gene disrupted clones we used a high-throughput method described by Hansen et al. (2015) for determining viable cell density and culture viability. In brief, a dye master mix, containing 5 µg/mL Hoechst-33342 (Life Technologies), for staining of total cell population, and 0.4 µg/mL propidium iodide (Life Technologies), for staining of dead cells, was prepared in CD-CHO medium supplemented with 8 mM L-glutamine, and was transferred to a 96-well optical-bottom microplate (Greiner Bio-One, Frickenhausen, Germany) containing 3 µL of cell suspension in a total volume of 200 µL per well. After incubation at room temperature, the cells were imaged using the appropriate channels in Celígo Imaging Cell Cytometer (Nexcelom Bioscience, MA, USA). Culture supernatants were analyzed for glucose, lactate, glutamine, glutamate and ammonium using BioProfile 400 Plus (Nova Biomedical, Waltham, MA, USA) and for AAs as described in section 2.6. Cultures were sampled for RNA and intracellular proteins in mid-exponential growth phase. Genomic DNA was extracted to verify the culture genotype using sanger sequencing (Eurofins Genomics) at the end of the cultures.

2.5. Cell cultivation in bioreactors

Pre-cultures were handled as described for cultivation in shake flasks. Cell culture was performed in single-use bioreactors (Eppendorf DASbox Mini Bioreactor, Jülich, Germany) with a working volume of 250 mL. Cultures were seeded and sampled as described in section 2.4. Temperature was maintained at 37 °C, agitation rate was fixed at 200 rpm, dissolved oxygen was maintained at 50% of atmospheric air saturation using air, O_2 and CO_2 operated at a constant flow rate of 0.6 L/h. Culture pH was maintained at 7.15 with a deadband of 0.25 using intermittent CO_2 addition to the gas mix and 2 M sodium carbonate.

2.6. HPLC quantification of AAs

Supernatants were quantified for AAs using the method described by Valgepea et al., 2017, with the following modifications: AAs were derivatised in a HPLC autosampler (Dionex Ultimate 3000) and samples were injected into a Gemini C18 column (3 µm, 4.6 × 150 mm, Phenomenex PN: 00F-4439-E0) with a guard column (SecurityGuard Gemini C18, Phenomenex PN: AJO-7597). The HPLC gradient was 5-22% B from 0-9.5 min, kept at 22% B to 11 min, 22–35% B from 11-14 min, kept at 35% to 20 min, 35–60% B from 20-24.5 min, 24.5–25.5%–100% B, kept at 100% B to 27 min, decreased to 5% B at 27.1–30 min where chromatography finished. Buffer A was 40 mM Na_2HPO_4, 0.02% NaN_3 (w/v) at pH 7.8. Buffer B was 45% (v/v) acetonitrile, 45% (v/v) methanol and 10% (v/v) water. Flow rate was 1 mL/min from 0-26 min and 1.5 mL/min from 26.1-29 min thereafter 1 mL/min to 30 min. Derivatised AAs were monitored using a fluorescence detector. OPA-derivatised AAs were detected at 340ex and 450em nm and FMOC-derivatised AAs at 266ex and 305em nm. Quantifications were based on standard curves derived from serial dilutions of an in-house prepared mixed AA standard. The upper and lower limits of quantification were 75 and 0.5 µg/mL, respectively. Chromatograms were integrated using Chromeleon version 7.1.3.

2.7. Calculations and statistics

Maximum specific growth rate was calculated using exponential regression of viable CHO cell density from day 0 to day 3. Average specific production rates of lactate and ammonium were calculated during the time interval from day 0 to day 3, by dividing the increase in metabolite concentration by the increase in integral of viable cell density (IVCD). Similarly, specific consumption rates of AAs were determined from day 0 to day 3. For assessing differences in rates between gene edited and wildtype clones, Levene's test for means was used initially to test for homogeneity of variances. The statistical test for difference between clones was performed using Student's or Welch's *t*-test as appropriate, with significance level of $\alpha = 0.05$.

2.8. Preparation of DNA, RNA, cDNA and qPCR experiments

Genomic DNA (gDNA) was isolated from pellets of 0.5×10^6 CHO cells using QuickExtract DNA Extraction Solution (Epicentre, Madison, WI, USA). For DNA preparation, the cell pellet was homogenized by vortexing in 200 µL 65 °C preheated QuickExtract solution. The mixture was incubated at 65 °C for 15 min and 98 °C for 5 min and centrifuged at $5000 \times g$ for 3 min. The supernatant containing DNA was used for further experimentation.

Total RNA was extracted from at least 10^6 cells using Trizol reagent (Life Technologies #15596-026) according to the manufacturer's

description. For qPCR experiments, cDNA was prepared from 500 ng TURBO-DNase (Life Technologies #AM1907) treated RNA using the qScript Flex cDNA kit (Quanta Bioscience # 95049-100) with random priming. qPCR was performed in an Mx3005P (Agilent Technologies) using Brilliant III Ultra-Fast SYBR® Green master mix (Agilent Technologies # 600882). Primers for qPCR are listed in Supplementary Table 1. Relative gene expression levels were calculated using the ΔΔCT method with *Gapdh* as reference gene.

2.9. Sample preparation for proteomic analysis

Preparation of protein extract from CHO cells was done as previously described in Bonde et al. (2016). Liquid chromatography was performed on an Easy-nLC system (Thermo scientific) coupled to an 75 μm × 15 cm C18 easy spray column (Thermo Scientific). Using a stepped gradient, going from 6% to 60% acetonitrile in water over 120 min, the samples were sprayed into an Orbitrap Fusion mass spectrometer (Thermo Scientific). MS-level scans were performed with Orbitrap resolution set to 60,000; AGC Target 2.0e5; maximum injection time 50 ms; intensity threshold 5.0e3; dynamic exclusion 45 s. Data dependent MS2 selection was performed in Top Speed mode with HCD collision energy set to 28% and ion trap detection (AGC target 1.0e4, maximum injection time 35 ms). The resulting data were analyzed using MaxQuant with the following settings: Fixed modifications: Carbamidomethyl (C). Varible modifications: oxidation of methionine residues. First search mass tolerance 20 ppm and a MS/MS tolerance of 20 ppm. Trypsin was selected as enzyme and allowing one missed cleavage. FDR was set at 0.1%.

For gel-based proteomics, gel bands were excised from the gel and washed first in 50% acetonitrile followed by water. After drying, the spots were in-gel-digested overnight at 37 °C with trypsin as enzyme. Peptide containing samples were analyzed on a Synapt G2 (Waters, Manchester UK) Q-TOF instrument as previously described in Ørnholt-Johansson et al., 2017. RAW-files were analyzed using Progenesis QI for Proteomics version 2.0.

3. Results & discussion

3.1. Selection of AA catabolic genes for genome editing

The ideal metabolic engineering strategy should increase availability of AAs for proteogenesis, while reducing synthesis of toxic metabolites, as well as avoiding adverse effects on cellular maintenance processes. To achieve this, we carefully selected catabolic pathways in AA metabolism for targeted disruption based on three criteria: (i) Pathways must not be essential for cell survival. (ii) Pathways should include transaminases or dehydrogenases, as these biochemical reactions were hypothesized to contribute to production of ammonium and lactate, respectively. (iii) Pathways should preferably be upregulated in our network reconstruction of AA metabolism, which integrated differential gene expression data generated from an IgG producing cell line and a non-producing cell line. Hence, the dataset was assumed to reflect changes in gene expression levels as a direct response to recombinant protein production, and consequently should reveal which AA catabolic pathways contribute the most to energy metabolism, when exposed to the metabolic burden of recombinant protein production. We targeted genes encoding the first catabolic reaction in each pathway to avoid accumulation of potentially toxic pathway intermediates. In cases where the first catabolic reaction was performed by isoenzymes encoded by three or more genes, we decided to target the second catabolic reaction, to reduce the number of gRNAs needed to disrupt pathway activity.

When inspecting the gene expression landscape in AA catabolic pathways, we found that the L-tryptophan, L-lysine, L-phenylalanine and L-tyrosine catabolic pathways were upregulated in the IgG producing cell line (Fig. 1; the complete map is found in Supplementary Fig. 1), indicating that CHO cells increase catabolism of said AAs when producing recombinant proteins. To disrupt these pathways, we selected a total of four genes encoding catabolic enzymes for knock-down (Table 1). In addition to these genes, we selected five genes in catabolic pathways of L-glutamate, L-proline and L-threonine (Table 1), as these pathways contained dehydrogenases and/or transaminases, and thus were expected to reduce specific lactate and ammonium. All target genes were tested for lethality by simulating their disruption using the consensus genome-scale reconstruction of CHO cell metabolism (Hefzi et al., 2016), and found to be non-lethal when deleted.

3.2. Generation of single gene disruptions and characterization of clone genotypes

In order to disrupt the target genes (Table 1), we selected a Cas9-based strategy to generate indels in 5' proximal exons in the coding region of each target gene causing out-of-frame mutations leading to premature termination of translation and/or translation of non-functional peptides. In order to exclude the potential impact of simultaneous production of a heterologous protein, we disrupted genes in a non-producing cell line.

We evaluated four target sites and screened each gRNA for indel generation efficiency by PCR amplification and deep sequencing of the targeted genomic region. The most efficient (i.e. highest ratio of indel over wild type sequence) gRNA sequence was selected for co-transfection with GFP_2A_Cas9. An off-target effect prediction was made based on the CHO-K1 genome (Supplementary Table 2), and found to be specific for the target genes (at least 3 mismatches in off-target sequences for the gRNA). We enriched transfected cell pools for cells expressing GFP-linked Cas9 nuclease using FACS, which has previously been shown to dramatically increase the indel frequency and thus reduce downstream clone screening efforts (Grav et al., 2015). We characterized single cell sorted clones for indels in target loci using PCR amplification and deep sequencing. The deep sequencing identified a set of clones with indels disrupting the genes of interest (Indel sizes found in Table 1), which were selected for further analysis (Henceforth named based on the disrupted genes).

3.3. Molecular characterization of gene disruption

Introduction of targeted frame-shift mutations in genes has been shown to effectively disrupt the activity of encoded proteins in CHO cells (Grav et al., 2015; Ronda et al., 2014), leading to translation of non-functional and/or truncated target proteins. We chose to examine the molecular effect of the disruption at both RNA and protein level.

As the mutation is introduced in the coding region, the promoter activity is assumed to be unaffected by the mutation. Indeed, we detected active transcription of all genes using qPCR, except for *Prodh2*, which was not expressed at detectable levels in the potential gene disruption clone (Fig. 2). However, we found that most genes were transcribed at a lower level in potential gene disruption clones than the wild type (Fig. 2), suggesting that the gene editing affected mRNA stability. Nonsense-mediated mRNA decay (NMD) is a cellular quality control system that prevents translation of dysfunctional proteins by degrading mRNAs with premature stop codons (reviewed by Lykke-Andersen and Jensen, 2015), and thus offer an explanation to the observed decrease in mRNA abundance. Assembly of the NMD complex on a premature stop codon induces endonucleolytic cleavage of the mRNA followed by decapping, deadenylation and complete mRNA cleavage by general 5′-3′ and 3′-5′ exonucleases. To investigate possible impact of NMD activity on our qPCR data, we decided to quantify mRNA abundance using two primer pairs located towards the 5′ and 3′ end of the coding region in each gene. For four genes (*Afmid, Ddc, Gad2* and *Prodh*) qPCR results indicated a difference in determined mRNA levels, suggesting a possible impact of NMD on the quantification of mRNA abundance (Fig. 2 and Supplementary Fig. 2), However, no clear trend

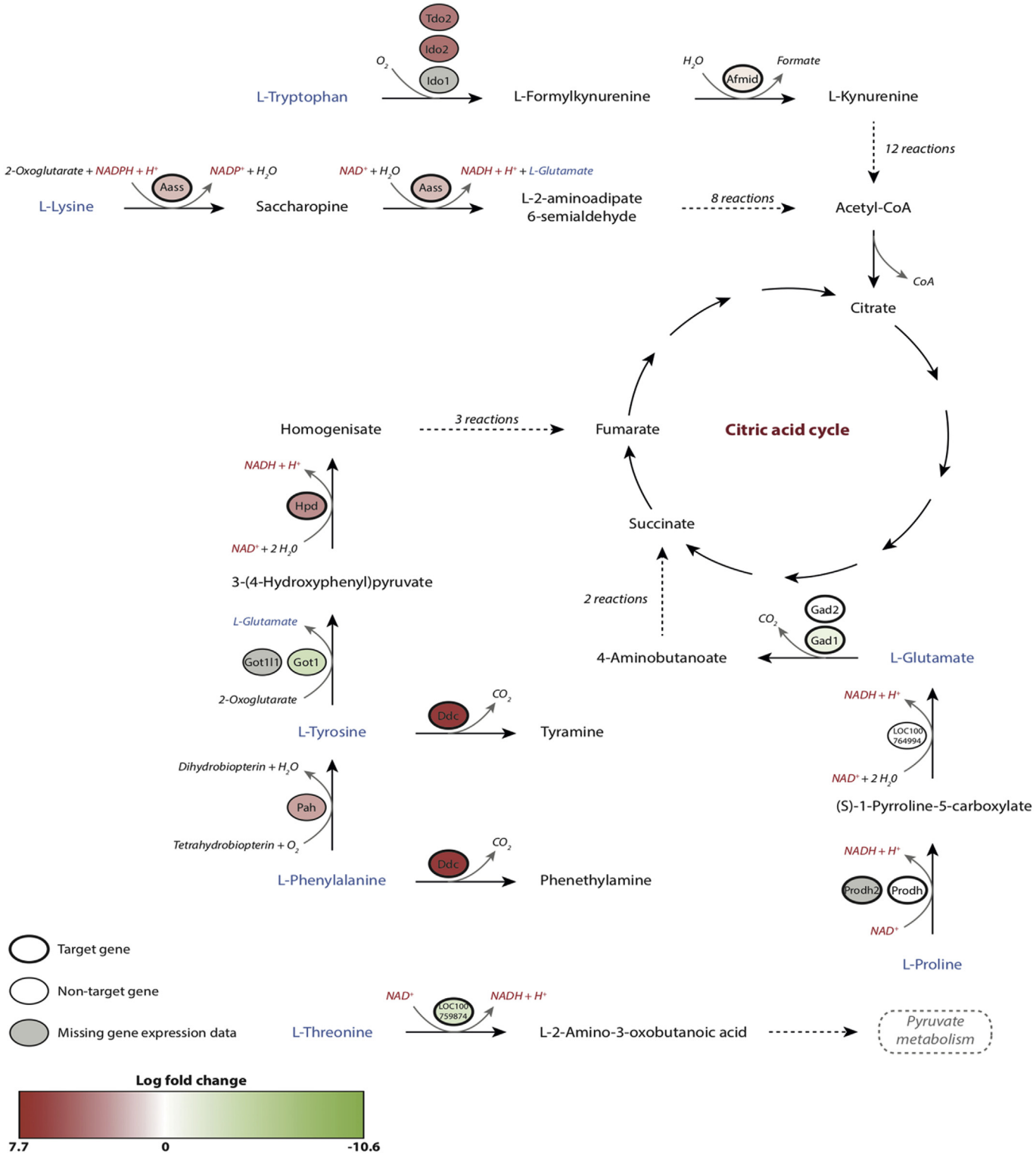

Fig. 1. Simplified overview of targeted AA catabolic pathways. Multiple reactions have been collapsed for simplicity. Circles next to reaction arrows indicate genes encoding the corresponding enzymes that catalyze each reaction. Circle colors indicate differential gene expression levels comparing an IgG producing cell line to a non-producing cell line (i.e. log fold-change [IgG/WT]). Grey circle color indicates missing gene expression data. AAs are colored blue, redox active compounds are colored red. We targeted the genes: Aass, Afmid, Ddc, Gad1, Gad2, Hpd, LOC100759874, Prodh and Prodh2, which are indicated with bold circles. (For interpretation of the references to color in this figure legend, the reader is referred to the Web version of this article.)

was observed for the 3′ versus 5′ end of the transcripts.

We further attempted to characterize target proteins using LC-MS/MS, and while we detected 2900 proteins in total, but target protein levels were below the detection limit (data not shown).

In summary, the deep sequencing shows correct disruption of the genes (Table 1), and a follow-up qPCR analysis of transcript levels showed that most genes additionally have a knock-down effect at the transcriptional level (Fig. 1), in the non-functional transcript.

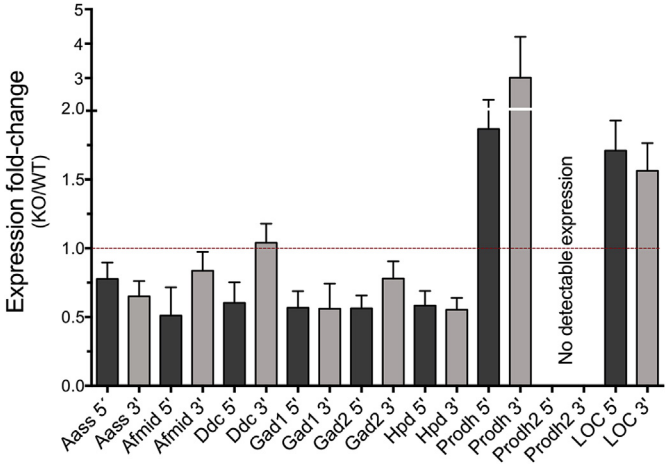

Fig. 2. Gene expression levels of target genes in single gene disrupted clones. Transcription rate was quantified using two primer pairs targeting coding regions upstream and downstream relative to the gRNA target site. Gene expression levels are normalized to the wild type expression. Error bars indicate standard deviation of three biological replicates.

3.4. Physiological characterization of single gene disrupted clones

To investigate potential improvement in bioprocessing potential derived from disrupting AA catabolic pathways in CHO cells, we performed a physiological comparison of nine gene-disrupted clones (genotypes in Table 1) with unedited wildtype cells as control. We monitored changes in growth (i.e. μ_{max} and IVCD) and specific metabolic by-product secretion (i.e. q_{Lac} and q_{NH3}) between the gene-disrupted clones and the control in batch culture performed in three separate shake flask experiments.

As presented in Fig. 3, the distribution of growth curves indicated a strong biological response to disruption of single AA catabolic genes, seen by increased maximal viable cell density, in comparison to wild type control, in clonal cell lines where the following genes were disrupted: *Aass, Afmid,* and *Hpd* (Fig. 3A); *Gad2* and LOC100759874 (Fig. 3B); and *Prodh* (Fig. 3C). Additionally, in comparison to the control cell line, eight of nine gene-disrupted clones displayed increased mean μ_{max}, up to 115% of the wild type μ_{max} (Fig. 4). The mean IVCD was increased in 6 of 9 clones up to 136% of wild type IVCD. For specific secretion of metabolic by-products, we found that single gene disruptions decreased mean q_{Lac} in 4 of 9 clones (up to 119% of wild type rate, highlighting the connection between lactate and AA metabolism (Nicolae et al., 2014)). Similarly, mean q_{NH3} was decreased in 5 of 9 clones to 91% of wild type rate, indicating a decrease in transamination associated with AA catabolism.

When comparing the physiological impact of each gene disruption individually, we found that some gene disruptions produced statistically significant (*t*-test, $\alpha < 0.05$) improvements across multiple investigated parameters (i.e. increased μ_{max} and IVCD and reduced q_{Lac} and q_{NH3}), while other disruptions produced minor, but statistical insignificant improvements (Fig. 4). Of particular interest was the *Hpd*-disrupted clone, which improved in all investigated parameters, and the *Gad2*-disrupted clone, which improved in all parameters except q_{NH3} (for q_{NH3}, p-value was 0.08). Of lesser interest and effect were the other gene-disrupted clones, for instance the *Afmid*-disrupted clone which featured increased μ_{max} and IVCD, but with no significant change in specific by-product secretion (although for q_{NH3}, p-value was 0.08), while the *Aass*-disrupted and *Prodh*-disrupted clones featured increased μ_{max} and IVCD, respectively. These results highlighted the potential in engineering AA metabolism towards improved bioprocessing performance. To this end, improvement of IVCD is especially desirable, as it represents the cell-work-hours available for protein synthesis and is correlated to protein titer (Altamirano et al., 2004).

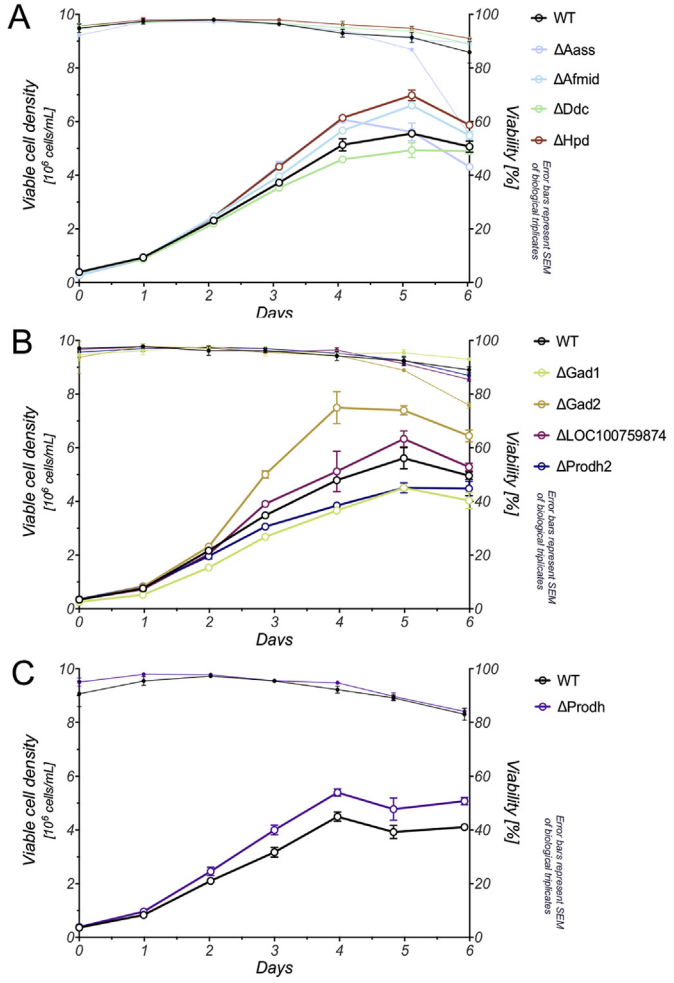

Fig. 3. Profile of cell growth and viability of single gene disruption clones and wild type cells. Growth curves were generated from three separate experiments where sets of clonal cell lines with disrupted single genes Aass, Afmid, Ddc, and Hpd (A), Gad1, Gad2, Prodh2, and LOC100759874 (B) and Prodh (C) were cultivated in parallel with CHO-S cells ("WT"). Error bars indicate SEM calculated for three biological replicates.

Notably, we found that the reductions of specific lactate and ammonium secretion in the gene edited clones were generally not reflected in absolute concentrations of the by-products in the culture medium (Fig. 5). Only the *Hpd* knock-down clone produced lower lactate concentration of about 2-3 mM on average throughout the culture compared to the control.

To our knowledge, this is the first study describing genome editing of AA metabolism at this scale in CHO cells, which complicates the comparison of our results to other studies. However, medium optimization studies offer insight into the physiological response to various AA concentrations and associated uptake rates. Previous reports have demonstrated that availability of AAs above a certain threshold inhibits cell growth (Chen and Harcum, 2005; Parampalli et al., 2007), as excess AA availability increase AA catabolism, which result in accumulation of associated growth inhibiting compounds (Mulukutla et al., 2017, 2019). Our observations are consistent with these reports. For example, I. J. González-Leal et al. (2011) found that threonine had a negative effect on growth rate. In agreement with this, we found that disruption of the first gene in threonine catabolism, LOC100759874, increased mean μ_{max} and IVCD indicating that threonine catabolism may produce growth inhibiting compounds. Furthermore, Mulukutla et al., 2019 found that phenylalanine, tyrosine and tryptophan catabolism inhibit growth. Our results are consistent with this, as disruption of genes in

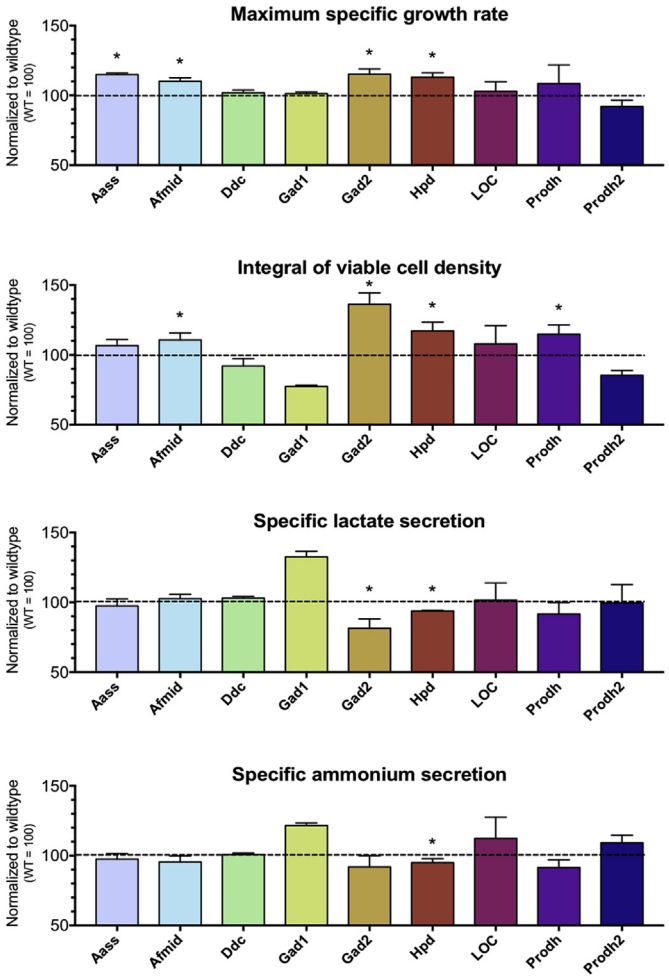

Fig. 4. Comparison of maximum specific growth rate, integral of viable cell density, specific lactate and ammonium secretion across nine gene disruption clones. Values have been normalized to the wild type. Stars indicate statistically significant difference to the wild type. Error bars indicate standard deviation of three replicates.

phenylalanine/tyrosine and tryptophan catabolism, *Hpd* and *Afmid*, respectively, significantly improved μ_{max} and IVCD. We found that disrupting *Aass* significantly increased μ_{max}, indicating that lysine catabolism is associated with growth inhibition. Mammalian *Aass* encodes a mitochondrial alpha-aminoadipic semialdehyde synthase, a bifunctional enzyme catalyzing the first two steps in the main catabolic pathway of lysine, the saccharopine pathway (Pena et al., 2016). The pathway produces reactive aldehydes, which are potentially toxic, as they form adducts and condensation products with proteins and DNA (Hallen et al., 2013), which may explain the observed growth benefit. *Gad1* and *Gad2* encode the isoenzymes glutamate decarboxylase 1 and 2, respectively (Erlander and Tobin, 1991), which catalyze the first reaction in glutamate degradation through a three-step anaplerotic pathway that leads to succinate (Supplementary Fig. 1). To our surprise, disrupting *Gad1* and *Gad2* had different effects in all physiological parameters (Fig. 4). In rats, *Gad1* and *Gad2* are both involved in γ-aminobutyric acid (GABA) synthesis and are expressed in distinct subcellular locations of the rat neuronal tissues. Immunochemical analysis suggest that *Gad1* is expressed in cell bodies and dendrites, while *Gad2* is predominantly expressed in nerve endings (Erlander and Tobin, 1991), indicating that subcellular location may explain the different physiological effect of disrupting *Gad1* and *Gad2*. However, the subcellular location of these proteins in CHO cells has not yet been determined. *Prodh* and *Prodh2* encode isoenzymes that catalyze the first catabolic reaction in degradation of proline to glutamate; a catabolic pathway consisting of two reactions (Supplementary Fig. 1). Both enzymes localize to the mitochondria in mouse (Cruz et al., 2003; Pagliarini et al., 2008), suggesting that the enzymes localize to the mitochondria in CHO cells as well. Still, we found that disrupting *Prodh* and *Prodh2* produced different responses in all physiological parameters (Fig. 4), despite the apparent similar catalytic function of the enzymes, suggesting that they are not isoenzymes in a functional sense, but rather structurally similar enzymes.

3.5. Evaluation of amino acid consumption rates in Gad2-and Hpd-disrupted clones

As the analysis showed above, the two most interesting phenotypes were found in the *Gad2*-and *Hpd*-disrupted clones. To further investigate the impact of these disruptions, we measured AA uptake rates by AA quantification in culture. We did not find any statistically significant difference (*t*-test, $\alpha < 0.05$) in specific AA uptake rates between gene edited clones and wild type, suggesting that these AAs are primarily utilized for protein synthesis instead of catabolism in the mutants (Supplementary Tables 3–4). Additionally, the fact that AA uptake rates remained unchanged enables straight-forward engineering of AA catabolism in existing production cell lines, since requirements for bioprocess adaptation upon engineering are minimal.

3.6. Physiological characterization and validation of physiological effect across multiple Gad2-or Hpd-disrupted clones

Functional heterogeneity in CHO cell populations, also known as clonal variation, is a general challenge in CHO cell engineering. To exclude that the improved phenotype observed in gene disrupted CHO clones was caused by random clonal variation, we characterized five clones with either *Gad2* or *Hpd* disrupted, as these gene disruptions had the biggest physiological effect and thus the most interesting leads. The clones were generated together with the single gene-disrupted clones described above, and had all disrupting indels (Table 2). The five clones and wild type were subjected to a similar physiological characterization as the clones above, including growth characterization (Fig. 6 and Table 2), and amino acid consumption rates (Supplementary Tables 6 and 7). In summary, these biological replicates all confirm the phenotypes seen above. While standard deviations vary across μ_{max}, IVCD, q_{Lac}, and q_{NH3} determinations, numerical changes are generally significant: All gene-edited clones had increased μ_{max}. For △*Gad2*, the increase was 1-13%, and for △*Hpd* 11–19%. IVCD reflected this; due to initially larger growth rates, IVCD increased by 9-50% (△*Gad2*) and 20–50% for △*Hpd*. Specific productivities generally dropped relative to the wildtype. q_{Lac} dropped up to 22% in △*Gad2* #2 (although △*Gad2* #1 showed marginally increased q_{Lac}) and dropped by 12-22% in △Hpd cell lines. Ammonium production was generally decreased by 3-26% (△*Gad2*) and 7–17% (△*Hpd*). The general variation in the effects highlights the importance of characterizing multiple clones when performing metabolic engineering of CHO cells due to clonal variation.

4. Conclusion

In summary, our results shows that growth improvements can be achieved from disrupting single AA catabolic pathways. In particular, disruption of *Hpd* and *Gad2* had desirable phenotypes for growth rate, IVCD, q_{NH3}, *and* q_{lac}.

Conflicts of interest

The authors state that D.L, H.F.K, and M.R.A have filed patent no.: WO2017EP70682, addressing some of the findings of this manuscript. The remaining authors have no conflicts of interest.

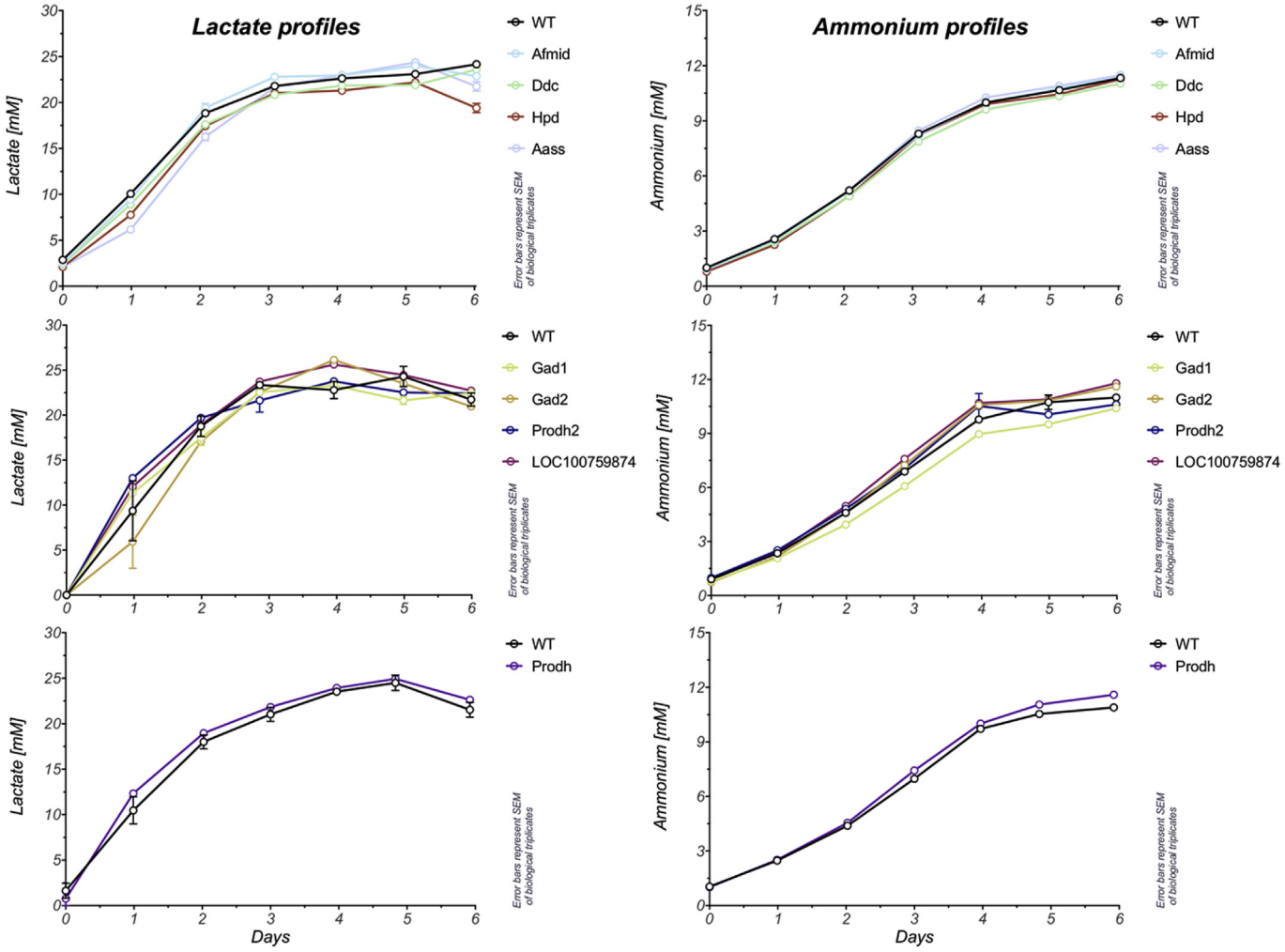

Fig. 5. Extracellular metabolite profiles of lactate and ammonium in single gene disruption clones and wild type. Data were generated in three separate experiments in biological triplicates. Cells were cultured in parallel with un-modified CHO-S cells ("WT"). Error bars indicate SEM. Note that error bars for some data bars appear to be missing, they are very close to 0 and hidden by the marker.

Declaration of interests

The authors declare no competing interests.

Grant numbers

The Novo Nordisk Foundation and eCHO Systems H2020 MSC-ITN (Grant no. 642663) provided funding for this work.

Author contributions

D.L, S.P., H. F. K. and M.R.A. designed experiments and wrote the manuscript. D.L., S.P., T.K.H. & T.W performed the experiments. H.H. validated essentiality of target genes. A.M.L. provided differential gene expression data. D.L., S.P., L.E.P., J.A., T.W., H.F.K. and M.R.A. analyzed the data. All authors reviewed the manuscript.

Acknowledgements

We acknowledge Karen Katrine Brøndum and Zufiya Sukhova for technical assistance with generation of genome edited cell lines. Moreover, we thank Sara Bjørn Petersen for cloning plasmids and Thomas Beuchert Kallehauge for sharing his experience in design of quantitative PCR experiments, Lene Holberg Blicher for assisting in the proteomics experiment, Mette Kristensen and Lars Boje Petersen for assisting in the HPLC analysis. The Novo Nordisk Foundation and eCHO Systems H2020 MSC-ITN (Grant no. 642663) provided funding for this work.

Table 2
Comparison of growth characteristics (μ_{max} and IVCD), by-product secretion rates (q_{NH3} and q_{Lac}) and indel sizes in respective target genes across wildtype, *Hpd*- and *Gad2*-disrupted clones. Values represent mean ± one standard deviation of three biological replicates.

	Wildtype	△*Gad2* #1	△*Gad2* #2	△*Gad2* #3	△*Hpd* #1	△*Hpd* #2
μ_{max} (*Day*$^{-1}$)	0,89 ± 0,13	0,9 ± 0,1	0,97 ± 0,11	1,01 ± 0,12	0,99 ± 0,21	1,06 ± 0,16
q_{NH3} (pmol/cell/day)	1,2 ± 0,2	1,16 ± 0,25	0,89 ± 0,17	1,03 ± 0,26	1,12 ± 0,13	1 ± 0,11
q_{Lac} (pmol/cell/day)	4,29 ± 1,03	4,37 ± 1,05	3,25 ± 0,62	3,34 ± 0,85	3,68 ± 0,49	3,77 ± 0,56
IVCD (10^6 cell*h/mL)	598,89 ± 9,26	649,65 ± 43,77	835,7 ± 35,01	897,43 ± 31,83	717,01 ± 57,55	759,41 ± 29,94
Indel size	–	-7	-25	-13	+1	+1

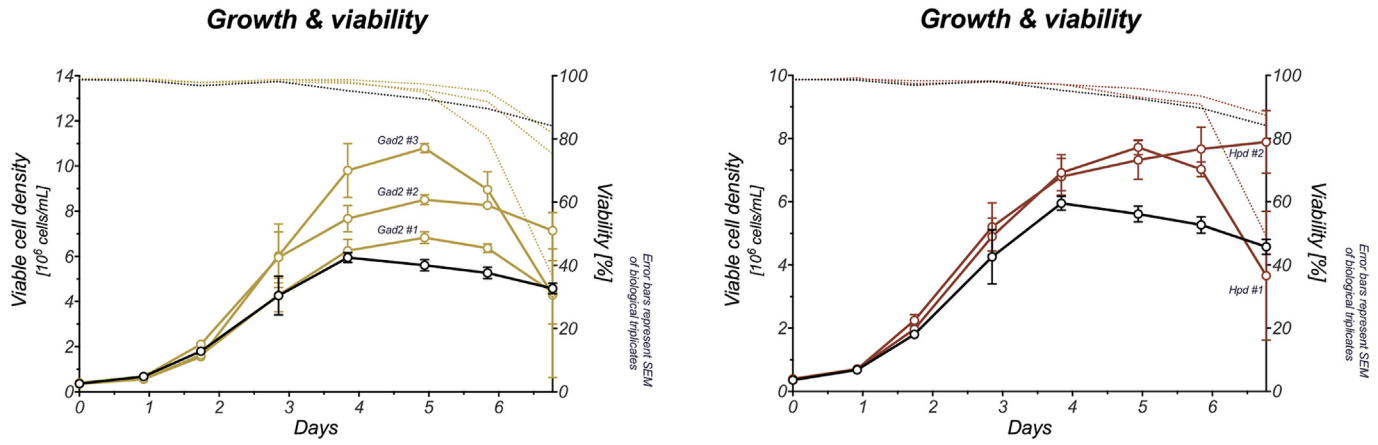

Fig. 6. Growth and viability of multiple Gad2 (Left) and Hpd (Right) disrupted clones and wild type cells. Growth curves were generated from the cultivation of multiple clonal cell lines with disrupted single genes Gad2 (left) and Hpd (right) were cultivated in parellel with CHO-S wild type cells. Error bars indicate SEM calculated for three biological replicates. Note that error bars for some data bars appear to be missing, they are very close to 0 and hidden by the marker.

Appendix A. Supplementary data

Supplementary data to this article can be found online at https://doi.org/10.1016/j.ymben.2019.09.005.

References

Ahn, W.S., Antoniewicz, M.R., 2012. Towards dynamic metabolic flux analysis in CHO cell cultures. Biotechnol. J. 7, 61–74. https://doi.org/10.1002/biot.201100052.

Altamirano, C., Berrios, J., Vergara, M., Becerra, S., 2013. Advances in improving mammalian cells metabolism for recombinant protein production. Electron. J. Biotechnol. 16, 1–16. https://doi.org/10.2225/vol16-issue3-fulltext-2.

Altamirano, C., Paredes, C., Illanes, A., Cairó, J.J., Gòdia, F., 2004. Strategies for fed-batch cultivation of t-PA producing CHO cells: substitution of glucose and glutamine and rational design of culture medium. J. Biotechnol. 110, 171–179. https://doi.org/10.1016/j.jbiotec.2004.02.004.

Anders, S., Pyl, P.T., Huber, W., 2015. HTSeq-a Python framework to work with high-throughput sequencing data. Bioinformatics 31, 166–169. https://doi.org/10.1093/bioinformatics/btu638.

Andersen, D.C., Goochee, C.F., 1995. The effect of ammonia on the O-linked glycosylation of granulocyte colony-stimulating factor produced by Chinese hamster ovary cells. Biotechnol. Bioeng. 47, 96–105. https://doi.org/10.1002/bit.260470112.

Beltrán-Valero de Bernabé, D., Peterson, P., Luopajärvi, K., Matintalo, P., Alho, a, Konttinen, Y., Krohn, K., Rodríguez de Córdoba, S., Ranki, a, 1999. Mutational analysis of the HGO gene in Finnish alkaptonuria patients. J. Med. Genet. 36, 922–923.

Bonde, M.T., Pedersen, M., Klausen, M.S., Jensen, S.I., Wulff, T., Harrison, S., Nielsen, A.T., Herrgård, M.J., Sommer, M.O.A., 2016. Predictable tuning of protein expression in bacteria. Nat. Methods 13, 233.

Borys, M.C., Linzer, D.I., Papoutsakis, E.T., 1994. Ammonia affects the glycosylation patterns of recombinant mouse placental lactogen-I by Chinese hamster ovary cells in a pH-dependent manner. Biotechnol. Bioeng. 43, 505–514. https://doi.org/10.1002/bit.260430611.

Chen, P., Harcum, S.W., 2005. Effects of amino acid additions on ammonium stressed CHO cells. J. Biotechnol. 117, 277–286. https://doi.org/10.1016/j.jbiotec.2005.02.003.

Cruz, S. Da, Xenarios, I., Langridge, J., Vilbois, F., Parone, P.A., Martinou, J., 2003. Proteomic analysis of the mouse liver mitochondrial inner membrane 278. pp. 41566–41571. https://doi.org/10.1074/jbc.M304940200.

Erlander, M.G., Tobin, A.J., 1991. Two genes encode distinct glutamate decarboxylases 7. pp. 91–100. https://doi.org/10.1016/0896-6273(91)90077-D.

González-Leal, I.J., Carrillo-Cocom, L.M., Ramírez-Medrano, A., López-Pacheco, F., Bulnes-Abundis, D., Webb-Vargas, Y., Alvarez, M.M., 2011. Use of a Plackett-Burman statistical design to determine the effect of selected amino acids on monoclonal antibody production in CHO cells. Biotechnol. Prog. 27, 1709–1717. https://doi.org/10.1002/btpr.674.

Grav, L.M., Lee, J.S., Gerling, S., Beuchert Kallehauge, T., Holmgaard Hansen, A., Kol, S., Lee, G.M., Ebdrup Pedersen, L., Faustrup Kildegaard, H., 2015. One-step generation of triple knockout CHO cell lines using CRISPR Cas9 and fluorescent enrichment. Biotechnol. J. https://doi.org/10.1002/biot.201500027.

Hallen, A., Jamie, J.F., Cooper, A.J.L., 2013. Lysine metabolism in mammalian brain: an update on the importance of recent discoveries. Amino Acids 45, 1249–1272. https://doi.org/10.1007/s00726-013-1590-1.

Hammond, S., Kaplarevic, M., Borth, N., Betenbaugh, M., Lee, K., 2012. Chinese hamster genome database: an online resource for the CHO community at. Biotechnol. Bioeng. 109, 1353–1356. www.CHOgenome.org.

Hansen, H.A., Emborg, C., 1994. {I}nfluence of ammonium on growth, metabolism, and productivity of a continuous suspension {C}hinese hamster ovary cell culture. Biotechnol. Prog. 10, 121–124. https://doi.org/10.1021/bp00025a014.

Hansen, H.G., Nilsson, C.N., Lund, A.M., Kol, S., Grav, L.M., Lundqvist, M., Rockberg, J., Lee, G.M., Andersen, M.R., Kildegaard, H.F., 2015. Versatile microscale screening platform for improving recombinant protein productivity in Chinese hamster ovary cells. Sci. Rep. 5, 18016. https://doi.org/10.1038/srep18016.

Hefzi, H., Ang, K.S., Hanscho, M., Borth, N., Lee, D., Lewis, N.E., 2016. Article a consensus genome-scale reconstruction of Chinese hamster ovary cell metabolism article a consensus genome-scale reconstruction of Chinese hamster ovary. Cell Metabol. 434–443. https://doi.org/10.1016/j.cels.2016.10.020.

Hiller, G.W., Mulukutla, B.C., 2017. US20170107552A1: Method of Cell Culture.

Hiller, G.W., Mulukutla, B.C., 2015. Method of Cell Culture. WO 2015/140708 A1.

Ihaka, R., Gentleman, R., 1996. R: a language for data analysis and graphics. J. Comput. Graph. Stat. 5, 299. https://doi.org/10.2307/1390807.

Kanehisa, M., Goto, S., 2000. KEGG: kyoto encyclopedia of genes and genomes. Nucleic Acids Res. 28, 27–30.

Kim, D., Pertea, G., Trapnell, C., Pimentel, H., Kelley, R., Salzberg, S.L., 2013. TopHat2: accurate alignment of transcriptomes in the presence of insertions, deletions and gene fusions. Genome Biol. 14 R36. https://doi.org/10.1186/gb-2013-14-4-r36.

Langmead, B., Trapnell, C., Pop, M., Salzberg, S.L., 2009. Ultrafast and memory-efficient alignment of short DNA sequences to the human genome. Genome Biol. 10 R25. https://doi.org/10.1186/gb-2009-10-3-r25.

Lao, M.S., Toth, D., 1997. Effects of ammonium and lactate on growth and metabolism of a recombinant Chinese hamster ovary cell culture. Biotechnol. Prog. 13, 688–691. https://doi.org/10.1021/bp9602360.

Ley, D., Seresht, A.K., Engmark, M., Magdenoska, O., Nielsen, K.F., Kildegaard, H.F., Andersen, M.R., 2015. Multi-omic profiling of EPO-producing Chinese hamster ovary cell panel reveals metabolic adaptation to heterologous protein production. Biotechnol. Bioeng. 112, 2373–2387. https://doi.org/10.1002/bit.25652.

Lund, A.M., Kaas, C.S., Brandl, J., Pedersen, L.E., Kildegaard, H.F., Kristensen, C., Andersen, M.R., 2017. Network reconstruction of the mouse secretory pathway applied on CHO cell transcriptome data. BMC Syst. Biol. 11, 37. https://doi.org/10.1186/s12918-017-0414-4.

Lykke-Andersen, S., Jensen, T.H., 2015. Nonsense-mediated mRNA decay: an intricate machinery that shapes transcriptomes. Nat. Rev. Mol. Cell Biol. 16, 665–677. https://doi.org/10.1038/nrm4063.

Mulukutla, B., Kale, J., Kalomeris, T., Jacobs, M., Hiller, G., et al., 2017. Identification and control of novel growth inhibitors in fed-batch cultures of Chinese hamster ovary cells. Biotechnology and Bioengineering In press. https://doi.org/10.1002/bit.26313.

Mulukutla, B.C., Mitchell, J., Geoffroy, P., Harrington, C., Krishnan, M., Kalomeris, T., Morris, C., Zhang, L., Pegman, P., Hiller, G.W., 2019. Metabolic engineering of Chinese hamster ovary cells towards reduced biosynthesis and accumulation of novel growth inhibitors in fed-batch cultures. Metab. Eng. 54, 54–68. https://doi.org/10.1016/j.ymben.2019.03.001.

Nicolae, A., Wahrheit, J., Bahnemann, J., Zeng, A.-P., Heinzle, E., 2014. Non-stationary 13C metabolic flux analysis of Chinese hamster ovary cells in batch culture using extracellular labeling highlights metabolic reversibility and compartmentation. BMC Syst. Biol. 8, 50. https://doi.org/10.1186/1752-0509-8-50.

Ørnholt-Johansson, G., Frosch, S., Gudjónsdóttir, M., Wulff, T., Jessen, F., 2017. Muscle Protein Profiles Used for Prediction of Texture of Farmed Salmon (*Salmo salar* L.). Journal of Agricultural and Food Chemistry.

Pagliarini, D.J., Calvo, S.E., Chang, B., Sheth, S.A., Vafai, S.B., Ong, S., Walford, G.A., Sugiana, C., Boneh, A., Chen, W.K., Hill, D.E., Vidal, M., Evans, J.G., Thorburn, D.R., Carr, S.A., Mootha, V.K., 2008. A mitochondrial protein compendium elucidates complex I disease biology. https://doi.org/10.1016/j.cell.2008.06.016 112, 123.

Parampalli, A., Eskridge, K., Smith, L., Meagher, M.M., Mowry, M.C., Subramanian, A., 2007. Developement of serum-free media in CHO-DG44 cells using a central composite statistical design. Cytotechnology 54, 57–68. https://doi.org/10.1007/

s10616-007-9074-3.
Pena, I.A., Marques, L.A., Laranjeira, A.B.A., Yunes, J.A., Eberlin, M.N., Arruda, P., 2016. Simultaneous detection of lysine metabolites by a single LC – MS/MS method : monitoring lysine degradation in mouse plasma. SpringerPlus 1–9. https://doi.org/10.1186/s40064-016-1809-1.
Robinson, M.D., McCarthy, D.J., Smyth, G.K., 2010. edgeR: a Bioconductor package for differential expression analysis of digital gene expression data. Bioinformatics 26, 139–140. https://doi.org/10.1093/bioinformatics/btp616.
Rodríguez, J.M., Timm, D.E., Titus, G.P., Beltrán-Valero De Bernabé, D., Criado, O., Mueller, H. a, Rodríguez De Córdoba, S., Peñalva, M. a, 2000. Structural and functional analysis of mutations in alkaptonuria. Hum. Mol. Genet. 9, 2341–2350.
Ronda, C., Pedersen, L.E., Hansen, H.G., Kallehauge, T.B., Betenbaugh, M.J., Nielsen, A.T., Kildegaard, H.F., 2014. Accelerating genome editing in CHO cells using CRISPR Cas9 and CRISPy, a web-based target finding tool. Biotechnol. Bioeng. 111, 1604–1616. https://doi.org/10.1002/bit.25233.
Sallée, M., Dou, L., Cerini, C., Poitevin, S., Brunet, P., Burtey, S., 2014. The aryl hydrocarbon receptor-activating effect of uremic toxins from tryptophan metabolism: a new concept to understand cardiovascular complications of chronic kidney disease. Toxins 6, 934–949. https://doi.org/10.3390/toxins6030934.
Templeton, N., Lewis, A., Dorai, H., Qian, E.A., Campbell, M.P., Smith, K.D., Lang, S.E., Betenbaugh, M.J., Young, J.D., 2014. The impact of anti-apoptotic gene Bcl-2Δ expression on CHO central metabolism. Metab. Eng. 25, 92–102. https://doi.org/10.1016/j.ymben.2014.06.010.
Thorens, B., Vassalli, P., 1986. Chloroquine and ammonium chloride prevent terminal glycosylation of immunoglobulins in plasma cells without affecting secretion. Nature 321, 618–620. https://doi.org/10.1038/321618a0.
Valgepea, K., Loi, K., Behrendorff, J., Lemgruber, R., Plan, M., Hudson, M., Köpke, M., Nielsen, L., Marcellin, E., et al., 2017. Metabolic engineering. https://doi.org/10.1016/j.ymben.2017.04.007. In press.
Walsh, G., 2018. Biopharmaceutical benchmarks 2018. Nat. Biotechnol. https://doi.org/10.1038/nbt.4305.
Xu, X., Nagarajan, H., Lewis, N.E., Pan, S., Cai, Z., Liu, X., Chen, W., Xie, M., Wang, W., Hammond, S., Andersen, M.R., Neff, N., Passarelli, B., Koh, W., Fan, H.C., Wang, Jianbin, Gui, Y., Lee, K.H., Betenbaugh, M.J., Quake, S.R., Famili, I., Palsson, B.O., Wang, Jun, 2011. The genomic sequence of the Chinese hamster ovary (CHO)-K1 cell line. Nat. Biotechnol. 29, 735–741. https://doi.org/10.1038/nbt.1932.
Yang, M., Butler, M., 2000. Effects of ammonia on (CHO) cell growth, erythropoietin production, and glycosylation. Biotechnol. Bioeng. 68, 370–380.
Young, J.D., 2013. Metabolic flux rewiring in mammalian cell cultures. Curr. Opin. Biotechnol. https://doi.org/10.1016/j.copbio.2013.04.016.